

UCLA

UCLA Previously Published Works

Title

Arabidopsis SWR1-associated protein methyl-CpG-binding domain 9 is required for histone H2A.Z deposition.

Permalink

<https://escholarship.org/uc/item/6wb6944w>

Journal

Nature communications, 10(1)

ISSN

2041-1723

Authors

Potok, Magdalena E
Wang, Yafei
Xu, Linhao
et al.

Publication Date

2019-07-01

DOI

10.1038/s41467-019-11291-w






Peer reviewed

ARTICLE

<https://doi.org/10.1038/s41467-019-11291-w>

OPEN

Arabidopsis SWR1-associated protein methyl-CpG-binding domain 9 is required for histone H2A.Z deposition

Magdalena E. Potok^{1,9}, Yafei Wang^{2,9} , Linhao Xu², Zhenhui Zhong^{1,2,3} , Wanlu Liu^{1,4}, Suhua Feng¹, Bilguudei Naranbaatar¹, Shima Rayatpisheh^{1,5,8} , Zonghua Wang^{3,6}, James A. Wohlschlegel⁵, Israel Ausin^{1,2}  & Steven E. Jacobsen^{1,7} 

Deposition of the histone variant H2A.Z by the SWI2/SNF2-Related 1 chromatin remodeling complex (SWR1-C) is important for gene regulation in eukaryotes, but the composition of the *Arabidopsis* SWR1-C has not been thoroughly characterized. Here, we aim to identify interacting partners of a conserved *Arabidopsis* SWR1 subunit ACTIN-RELATED PROTEIN 6 (ARP6). We isolate nine predicted components and identify additional interactors implicated in histone acetylation and chromatin biology. One of the interacting partners, methyl-CpG-binding domain 9 (MBD9), also strongly interacts with the Imitation SWItch (ISWI) chromatin remodeling complex. MBD9 is required for deposition of H2A.Z at a distinct subset of ARP6-dependent loci. MBD9 is preferentially bound to nucleosome-depleted regions at the 5' ends of genes containing high levels of activating histone marks. These data suggest that MBD9 is a SWR1-C interacting protein required for H2A.Z deposition at a subset of actively transcribing genes.

¹Department of Molecular, Cell and Developmental Biology, University of California, Los Angeles, Los Angeles, CA 90095, USA. ²Basic Forestry and Proteomics Center, Fujian Agriculture and Forestry University, Fuzhou 350002, China. ³State Key Laboratory of Ecological Pest Control for Fujian and Taiwan Crops, Fujian Agriculture and Forestry University, Fuzhou 350002, China. ⁴Zhejiang University-University of Edinburgh Institute, Zhejiang University School of Medicine, Hangzhou 310058, China. ⁵Department of Biological Chemistry, David Geffen School of Medicine, University of California, Los Angeles, Los Angeles, CA 90095, USA. ⁶Institute of Oceanography, Minjiang University, Fuzhou 350108, China. ⁷Howard Hughes Medical Institute, University of California, Los Angeles, Los Angeles, CA 90095, USA. ⁸Present address: Genomic Institute of the Novartis Research Foundation, 10675 John Jay Hopkins Dr., San Diego, CA 92121, USA. ⁹These authors contributed equally: Magdalena E. Potok, Yafei Wang. Correspondence and requests for materials should be addressed to I.A. (email: israel.ausin@gmail.com) or to S.E.J. (email: jacobsen@ucla.edu)

Chromatin dynamics plays a central role in regulating gene expression and has important implications in various cellular processes. The basic unit of chromatin is the nucleosome, which consists of 147 base-pairs (bp) of DNA wrapped around a histone octamer composed of two of each of the histones H2A, H2B, H3, and H4 (ref. 1). Cells contain chromatin remodeling complexes, which modulate the packaging, spacing, and composition of nucleosomes^{2,3}. The activity, targeting, and composition of remodeling complexes is tightly regulated to enable proper development of an organism^{2,3}.

The most highly conserved histone variant in eukaryotes is H2A.Z^{4–6}. H2A.Z is found at many genes, most often around transcription start sites (TSS), with a particular preference for the +1 nucleosome^{7–10}. The relationship between H2A.Z accumulation and transcription is complex. When present in the active genes of some organisms, the levels of H2A.Z at the TSS positively correlate with gene expression, typically when found together with H3/H4 acetylation, marks of active transcription^{10–13}. H2A.Z is nonetheless absent at the most highly expressed genes⁷ and is also localized around the TSS of repressed genes that are poised for activation in yeast and animals^{9,14–16}. Although the function of gene body methylation is unclear, one study in *Arabidopsis* suggests that a function of gene body DNA methylation may be to prevent H2A.Z deposition over housekeeping genes^{7,17}, while another study found no such evidence¹⁸. However, it is clear that an anti-correlation between H2A.Z and DNA methylation exists across diverse systems^{16,19–21}. In *Arabidopsis*, genes bearing high levels of gene body DNA methylation tend to be long and highly expressed, and show H2A.Z enrichment at their 5'-ends overlapping with activating histone modifications^{17,22–24}. By contrast, enrichment of H2A.Z over gene bodies (including high H2A.Z levels at the TSS) is typically found in shorter, weakly expressed genes involved in environmental/stress responses that are marked with H3K27me3 (refs. 17,22–25). Recently, levels of H3K27me3 were shown to be dependent on H2A.Z deposition in *Arabidopsis*^{23,26}. Together, these studies demonstrate that H2A.Z can participate in both activation and repression of gene expression, likely in concert with other factors and chromatin marks.

H2A.Z is deposited by the SWI2/SNF2-Related 1 (SWR1) complex, which involves the replacement of H2A-H2B dimers by H2A.Z-H2B dimers^{27–29}. In yeast, the SWR1 complex (SWR1-C) is composed of 14 subunits³⁰. In mammals, the structurally and functionally equivalent homolog of the yeast SWR1 complex, Snf2-Related CREBBP Activator Protein (SRCAP), is composed of 11 subunits, which are also conserved in yeast^{31–33}. Based on homology, *Arabidopsis* contains one or several orthologs of the 11 conserved subunits from the yeast and human SWR1/SRCAP complexes, respectively³⁴. Based on genetic and protein–protein interaction studies, several components have been validated as components of the *Arabidopsis* SWR1 complex, including PHOTOPERIOD-INDEPENDENT EARLY FLOWERING 1 (PIE1), the ATPase/scaffold subunit; ACTIN-RELATED PROTEIN 6 (ARP6); SERRATED LEAVES AND EARLY FLOWERING (SEF), the homolog of the yeast SWC6; and SWR1 complex subunit 2 (SWC2)^{35–37}. A recent pull-down study of the SWC6 subunit identified additional subunits of the *Arabidopsis* SWR1 complex in yeast and validated their interaction with SWR1 complex subunit 4 (SWC4)³⁸. Mutations in the genes encoding the SWR1 subunits share various phenotypes, with null mutations in the core catalytic subunit PIE1 producing the most severe phenotypes, including reduced size, loss of apical dominance, reduced fertility, and early flowering^{35–37,39–41}.

How the SWR1 complex is targeted across the genome remains unclear. Evidence suggests that H2A.Z localization around TSS in yeast is dependent on open chromatin and histone acetylation deposited by the Nucleosome acetyltransferase of H4 (NuA4)

complex^{8,42–46}. The SWR1-C and NuA4 complexes share four common members: SWC4, YEAST ALL1-FUSED GENE FROM CHROMOSOME 9 (YAF9), ACTIN-RELATED PROTEIN 4 (ARP4), and ACTIN 1 (ACT1)^{27–29,47–49}. Homologs of these four proteins are present in the mammalian TIP60 complex, which possesses the dual activities of acetylating histones and depositing H2A.Z^{31,50,51}. The *Arabidopsis* genome also contains homologs for many of the yeast NuA4 subunits; however, a functional link between histone acetylation and H2A.Z deposition is unclear⁵². YAF9 proteins are required for both the proper expression of *FLOWERING LOCUS C* (*FLC*) and H2A.Z acetylation at its regulatory regions, but not for H2A.Z deposition⁵³. Much more needs to be learned about the potential NuA4 complex in *Arabidopsis*, including its composition and genome-wide effects on H2A.Z deposition and modification. Although genome-wide localization of the SWR1 components is lacking in *Arabidopsis*, it has been reported that ARP6 and SWC4 directly bind their target locus *FLOWERING LOCUS T* (*FT*)³⁸; likewise, ARP6 and SWC6 bind directly to *FLC*³⁵.

In this study, we use the conserved ARP6 subunit as bait to analyze the composition of the *Arabidopsis* SWR1 complex. We identify *Arabidopsis* homologs of most of the conserved SWR1 complex components in yeast, as well as several additional interacting partners: MBD9, four of the seven members of the ALFIN1-LIKE family (AL4, AL5, AL6, AL7), and two components of the yeast NuA4 and *Arabidopsis* SAGA histone acetyltransferase complexes, TRANSCRIPTION-ASSOCIATED PROTEIN 1A AND 1B (TRA1A and TRA1B). Our data are consistent with a related study where ARP6-interacting proteins were identified using ARP6-TAP-tag purification followed by mass spectrometry⁵⁴. We focus on characterizing MBD9, a protein implicated in flowering time regulation⁵⁵. Using biochemical, genetic, and transcriptome analyses, we show that MBD9 interacts with the SWR1 complex in *Arabidopsis*, and is required for H2A.Z deposition at a subset of ARP6-dependent genes. Furthermore, immunoprecipitation of MBD9 followed by mass spectrometry (IP–mass spec) reveals its association with the ISWI chromatin remodeling complex, suggesting additional functions for MBD9. Genome-wide ChIP-seq analyses of MBD9 show that it localizes to nucleosome-depleted regions of active genes but does not influence open chromatin itself. MBD9 is thus an interacting partner of the *Arabidopsis* SWR1 complex required for H2A.Z deposition at a subset of actively transcribed genes.

Results

MBD9 controls flowering time via its interaction with SWR1 complex. To identify components of the SWR1 complex in *Arabidopsis*, we used the conserved ARP6 subunit of the SWR1 complex as bait. We generated the epitope-tagged ARP6 lines *pARP6:ARP6-3xFLAG* and *pARP6:ARP6-9xMYC*. Both lines complemented *arp6-1* mutants (Supplementary Fig. 1), indicating that epitope-tagged ARP6 is functional in vivo. To detect as many potential protein interactions as possible, we performed IP–mass spec in both FLAG- and MYC-tagged ARP6 lines using highly proliferating inflorescence tissue where levels of proteins are high. In all replicates (three biological replicates with two technical replicates each), we observed enrichment of the *Arabidopsis* homologs of most of the conserved yeast SWR1 complex components—ARP6, PIE1, RuvB-like protein 1 and 2 (RIN1, RIN2), ARP4, SWC4, SWC2, YAF9A, and SEF. This includes three of the four common subunits of the yeast NuA4 complex, ARP4, SWC4, and YAF9A (Table 1). Our experiment confirms previous well-characterized in vivo and in vitro interactions of ARP6 with PIE1 and SEF^{36–38}. We additionally identified two homologs of the yeast Tra1 proteins, subunits of the yeast NuA4 complex, TRA1A

Table 1 IP-mass spectrometry of ARP6

Protein	Annotation	ARP6-9xMYC				Wild type				ARP6-3xFLAG		Wild type	
		R1	R2	R3	R4	R1	R2	R3	R4	R1	R2	R1	R2
AT3G33520	ARP6	123	119	138	123	0	0	0	0	573	501	0	0
AT3G12810	PIE1	175	208	206	202	0	0	0	0	76	82	3	0
AT5G22330	RIN1	176	189	224	196	3	4	0	0	62	56	5	7
AT5G67630	RIN2	115	136	175	146	3	2	2	0	51	41	7	5
AT1G18450	ARP4	75	76	64	56	8	3	5	2	35	37	9	10
AT2G47210	SWC4	45	46	33	39	0	0	0	0	30	25	0	0
AT2G36740	SWC2	37	32	35	34	0	0	0	0	14	11	0	0
AT5G45600	YAF9A	25	19	20	21	0	0	0	0	13	12	0	0
AT5G37055	SEF	11	9	9	8	0	0	0	0	9	8	0	0
AT3G01460	MBD9	67	71	97	108	0	0	0	0	10	11	0	0
AT2G17930	TRA1A	84	94	117	117	0	0	0	0	31	25	0	0
AT4G36080	TRA1B	72	78	91	91	0	0	0	0	19	17	0	0
AT5G26210	AL4	2	3	2	2	0	0	0	0	0	0	0	0
AT5G20510	AL5	12	16	15	14	0	0	0	0	3	4	0	0
AT2G02470	AL6	5	6	4	5	0	0	0	0	2	0	0	0
AT1G14510	AL7	6	3	5	6	0	0	0	0	0	0	0	0

Spectral counts for ARP6-9xMyc and ARP6-3xFlag lines representing enriched genes over wild type. Source data are provided as Source Data file

and TRA1B. We also observed consistent enrichment for several interacting partners previously implicated in chromatin biology, MBD9 (refs. ^{55,56}) and AL4, AL5, AL6, and AL7, which recognize di- and trimethyl H3K4 histone marks⁵⁷. The interaction between ARP6 and MBD9 was further validated by co-immunoprecipitation (co-IP) in *Arabidopsis* flowers using an antibody raised against MBD9 (Fig. 1a). We then generated epitope-tagged MBD9 lines, *pMBD9:MBD9-3xFLAG* and *pMBD9:MBD9-9xMYC*. Both lines complemented *mbd9-3* mutants (Supplementary Fig. 2), indicating that the epitope-tagged MBD9 is functional in vivo. We performed IP-mass spec using floral tissue from both FLAG- and MYC-tagged MBD9 lines. In both experiments we observed enrichment of the SWR1 complex components PIE1, RIN1, ARP4, RIN2, SWC2, ARP6, SWC4, YAF9A, and SEF (Table 2). Interestingly, we also identified TRA1A and TRA1B, components of the NuA4 complex, as common interacting partners between ARP6 and MBD9. Additionally, in our MBD9 IP-mass spec we detected high enrichment of ISWI chromatin remodeling complex members that were not preferentially enriched among the ARP6-associated proteins.

To explore the genetic interaction between MBD9 and ARP6, we used the T-DNA mutants *arp6-1* and *mbd9-3* (refs. ^{35,39,40,55,56}). Both single mutants displayed an early flowering time phenotype (Fig. 1c) as described previously^{39,40,55}. The *mbd9-3* phenotype was less severe than that of *arp6-1*; *mbd9-3* plants were larger, with a leaf morphology that more closely resembled wild-type plants (Fig. 1b). The *mbd9-3* mutant plants also flowered slightly later than the *arp6-1* mutants under both long-day (LD) and short-day (SD) conditions (Fig. 1c). The *arp6-1 mbd9-3* double mutants had a more severe developmental phenotype than either of the single mutants, which resembled the strong phenotype of *pie1-2*, a mutant affecting the catalytic subunit of the SWR1 complex (Fig. 1b)^{35,37,58}. The stronger phenotype of the *arp6-1 mbd9-3* double mutant was also observed in a related study by Sijacic et al.⁵⁴. Despite the severe developmental phenotype, the double mutant had a similar flowering time to *arp6-1* under both LD and SD conditions; however, the time until anthesis (floral opening) was slightly shorter under SD growth conditions in the double mutant than the *arp6-1* mutant (Fig. 1c), most likely due to morphological defects present in the *arp6-1 mbd9-3* double mutant. These data suggest that, regarding flowering time, ARP6 is epistatic to MBD9 in both LD and SD conditions. Expression analysis of key

flowering time genes, *FLC* and *MADS AFFECTING FLOWERING 4 AND 5* (*MAF4* and *MAF5*), indicated that both the single mutants and the double mutant had a similar reduction of expression of these genes (Fig. 1d). Together, these results indicate that MBD9 and ARP6 act together in the same genetic pathway controlling flowering time as part of the SWR1 complex.

MBD9 is required for the deposition of H2A.Z. To investigate the role of MBD9 in H2A.Z deposition, we analyzed H2A.Z levels in *Arabidopsis* seedlings before the major developmental transition to flowering in order to minimize secondary effects in mutants. We performed western blot on total extracts, and observed the levels to decline in the mutants: wild type > *mbd9-3* > *arp6-1* > *arp6-1 mbd9-3* (Fig. 2a). To investigate the impact of H2A.Z loss on chromatin, we performed two replicates of H2A.Z ChIP-seq in wild type, *mbd9-3*, *arp6-1*, and *arp6-1 mbd9-3*, with H3 ChIP-seq as a control. Pearson correlation indicated a considerable overlap between the ChIP-seq replicates (Supplementary Fig. 3a). As with H2A.Z protein levels, we detected a sequential decrease in H2A.Z signal over H2A.Z peaks in wild type and over protein-coding genes as follows: wild type > *mbd9-3* > *arp6-1* > *arp6-1 mbd9-3* (Fig. 2b). By contrast, H3 levels were unchanged over these regions (Supplementary Fig. 3b). Using the MACS2 peak caller for each replicate (*q* value <0.01), we defined common H2A.Z differential regions for each genotype (Supplementary Methods). We surveyed the gene annotations in each differential region and identified genes that lost H2A.Z in the mutants compared to wild type: 2594 for *mbd9-3*, 12,222 for *arp6-1*, and 15,226 for *arp6-1 mbd9-3*. GO term enrichment for the three groups of genes yielded similar results, including post-embryonic development and protein modification, indicating that broad classes of genes were impacted by the loss of H2A.Z in MBD9 and ARP6 mutants (Supplementary Fig. 3c).

Comparison of the H2A.Z-depleted genes in each mutant revealed a high degree of overlap (Fig. 2c). A metaplot of H2A.Z occupancy over the different groups of genes revealed that: (1) although *mbd9-3* mutants had fewer genes that lost H2A.Z than *arp6-1*, the depletion of H2A.Z over *mbd9-3*-dependent loci was nearly as great as in *arp6-1* (Fig. 2d); (2), genes that lost H2A.Z in *arp6-1* and *arp6-1 mbd9-3* behaved similarly, with H2A.Z enrichment following the order: wild type > *mbd9-3* > *arp6-1* > *arp6-1 mbd9-3* (Fig. 2e, f). We also defined 782 genes that required both MBD9 and ARP6 for H2A.Z deposition (*arp6-1*

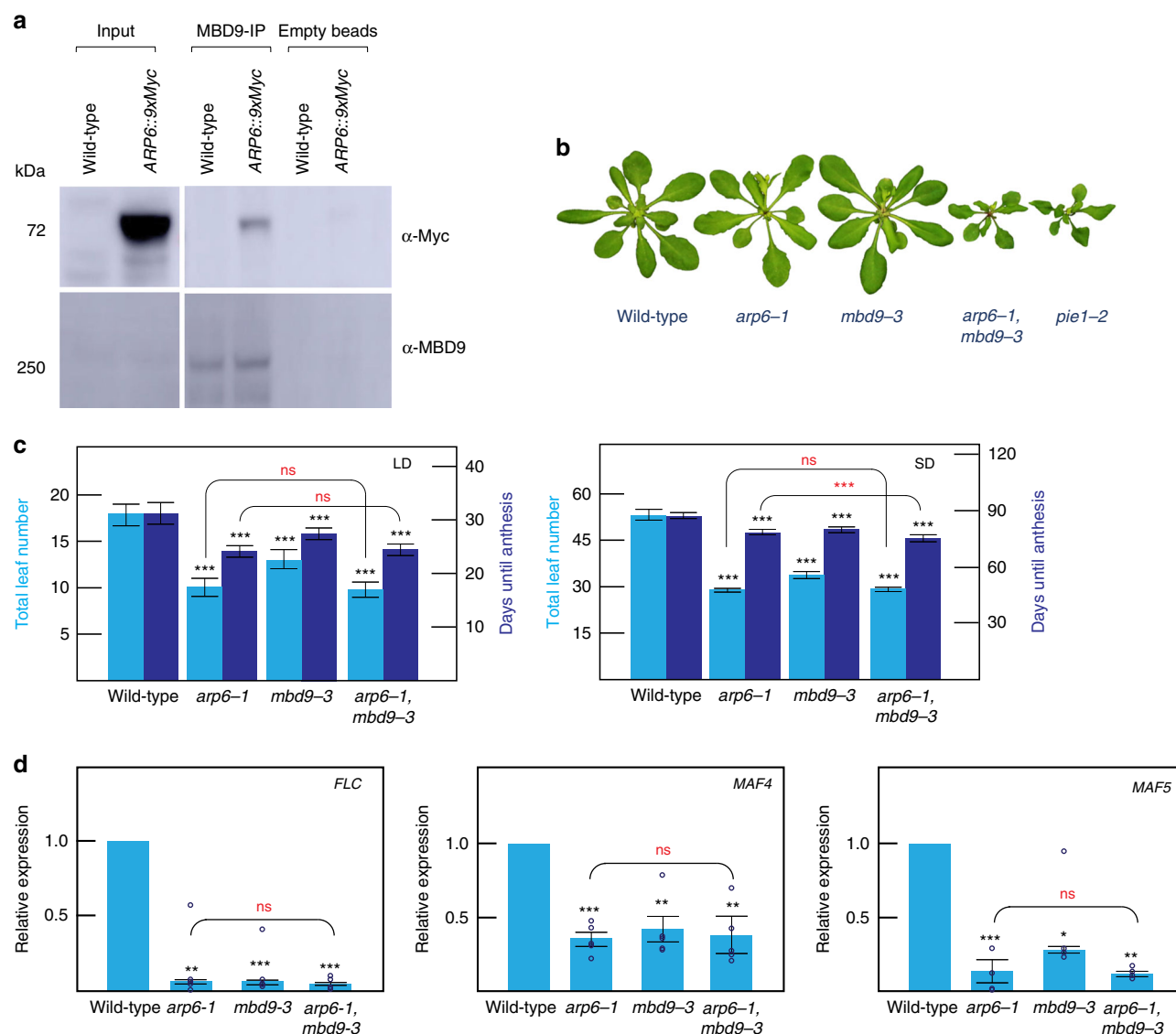


Fig. 1 ARP6 and MBD9 interaction and phenotype of the mutants. **a** Pull-down and co-immunoprecipitation assay. Empty bead lanes serve as negative controls. For each western blot, the antibody used is indicated to the right. **b** Phenotype of *arp6-1*, *mbd9-3*, *arp6-1 mbd9-3*, and *pie1-2* mutants. Plants were grown for 4 weeks (**b**) or 5 weeks (**c**) under long-day (LD) conditions (16 h light, 8 h dark) and short-day (SD) conditions (8 h light, 16 h dark). Flowering time expressed as the number of days from germination to anthesis as well as the total number of leaves produced by wild type, *arp6-1*, *mbd9-3*, and *arp6-1 mbd9-3* under the same conditions are shown. Averages from 16 plants \pm standard deviations are shown. Paired two-tailed Student's *t*-test was used to determine significance between wild type and mutants (black asterisks) or between mutants (red asterisks); ns *p* value > 0.05, **p* value \leq 0.05, ***p* value \leq 0.01, ****p* value \leq 0.001. **d** Relative expression levels of *FLC*, *MAF4*, and *MAF5* in wild type, *arp6-1*, *mbd9-3*, and *arp6-1 mbd9-3*. *UBQ10* was used as an internal control for expression analyses. Average expression levels from three independent replicates \pm standard deviations are shown. Paired two-tailed Student's *t*-test was used to determine significance between wild type and mutants (black asterisks) or between mutants (red asterisks); ns *p* value > 0.05, **p* value \leq 0.05, ***p* value \leq 0.01, ****p* value \leq 0.001. Source data for Figs. 1a, 1c, and 1d are provided as Source Data file

mbd9-3 mutant vs *arp6-1*, *q* value < 0.01). These genes were enriched for cell cycle progression functions (Supplementary Fig. 3c). The H2A.Z profiles over this set of genes (Fig. 2g) support the observation that these regions were dependent on both MBD9 and ARP6 for H2A.Z deposition. In *Arabidopsis*, housekeeping genes typically contain H2A.Z exclusively over the +1 nucleosome and lowly expressed/responsive genes contain H2A.Z over the entire gene bodies, with highest levels of H2A.Z at the TSS^{17,23,24}. To investigate which types of genes are most impacted by the loss of H2A.Z in our mutants, we divided genes (into nine classes) according to the levels of H2A.Z in wild type over gene bodies (low, medium, and high) and TSS (low, medium, and high) as described in ref. 17 (Supplementary Fig. 4, Supplementary Methods). We intersected these classes of gene

with genes that lost H2A.Z in our mutants and plotted their distribution (Fig. 2h). This revealed that loss of H2A.Z in the *mbd9-3* mutant tends to occur over genes possessing high levels of H2A.Z over the TSS and low levels of H2A.Z over gene bodies (HL class—High TSS, Low gene body), whereas loss of H2A.Z in the *arp6-1* mutant tends to occur over genes containing high levels of H2A.Z over gene bodies (LH, MH, and HH classes) (Fig. 2h).

MBD9/ARP6 partial redundancy in gene expression control.

To investigate the relationship between H2A.Z loss and transcription, we performed RNA-seq in seedlings in wild type, *mbd9-3*, *arp6-1*, and *arp6-1 mbd9-3*. We defined differentially

Table 2 IP-mass spectrometry of MBD9

Protein	Annotation	MBD9-9xMYC	MBD9-3xFLAG	Wild-type-9xMYC	Wild-type-3xFLAG
AT3G01460	MBD9	355	607	0	0
AT3G12810	PIE1	75	49	0	0
AT5G22330	RIN1	33	26	0	10
AT1G18450	ARP4	31	24	0	9
AT5G67630	RIN2	29	22	0	13
AT2G36740	SWC2	17	0	0	0
AT3G33520	ARP6	16	5	0	0
AT2G47210	SWC4	12	9	0	0
AT5G45600	YAF9A	5	6	0	0
AT5G37055	SEF	2	0	0	0
AT2G17930	TRA1A	128	76	0	0
AT4G36080	TRA1B	120	74	0	0
AT2G02470	AL6	2	0	0	0
AT5G18620	CHR17	122	190	0	3
AT3G0640	CHR11	118	177	0	4

Spectral counts for MBD9-9xMyc and MBD9-3xFlag lines representing enriched genes over wild type. Source data are provided as Source Data file

expressed genes (fold change >2, FDR <0.05, Supplementary Methods). We detected 277 misregulated genes in *mbd9-3*, 2042 in *arp6-1*, and 1620 in *arp6-1 mbd9-3*. Among the down-regulated genes we detected *FLC*, *MAF4*, and *MAF5* as targets of both MBD9 and ARP6, confirming our RT-qPCR results (Supplementary Fig. 5a). Importantly, the expression of genes encoding the predicted subunits of the SWR1 complex as well as H2A.Z genes were largely unaffected in the mutants (Supplementary Fig. 5b). We examined down-regulated and up-regulated genes (Fig. 3) and observed a high degree of overlap between the *arp6-1* and *arp6-1 mbd9-3* mutants, with 584 common up-regulated and 616 common down-regulated genes (Fig. 3a, b). These overlapping genes showed the same trend in expression change in *mbd9-3* mutants, but to a lesser degree that did not meet our significance cutoffs (Fig. 3c, d). We also defined genes specifically up- and down-regulated in either *mbd9-3* or *arp6-1*, implying independent functions at a subset of loci (Fig. 3a–d) as well as a set of 218 up-regulated genes that were dependent on both ARP6 and MBD9 for expression (Fig. 3a, c), suggesting a redundant role of MBD9 and ARP6 at this set of genes. By contrast, the unique down-regulated genes ($n = 170$) did not show a significant change between *arp6-1* and *arp6-1 mbd9-3* (Fig. 3b, d). GO term analysis indicated that up-regulated genes in *mbd9-3* mutants are involved in post-embryonic development and response to stress, whereas for *arp6-1* and *arp6-1 mbd9-3* up-regulated genes are involved in lipid localization, biosynthetic processes, and response to drug (Supplementary Fig. 5c). By contrast, down-regulated genes are involved in response to stress, stimulus, and defense in all mutants (Supplementary Fig. 5c).

We compared differentially expressed genes in relation to H2A.Z changes in the mutants. First, to obtain general trends, we generated boxplots of expression and profiles of H2A.Z in the nine classes of genes divided according to their H2A.Z occupancy (Supplementary Fig. 4) for wild type, *mbd9-3*, *arp6-1*, and *arp6-1 mbd9-3* (Supplementary Fig. 6a, b). One general trend stood out, genes containing high-medium H2A.Z levels over gene bodies and the highest H2A.Z levels over TSS showed increased expression upon loss of H2A.Z in *arp6-1*, which was even more pronounced in the *arp6-1 mbd9-3* mutant (Supplementary Fig. 6a, b). Only a weak loss of H2A.Z was observed in the *mbd9-3* mutant over these classes of genes where expression was not significantly increased (Supplementary Fig. 6a, b). Interestingly, looking at a typical H2A.Z profile of housekeeping genes (low H2A.Z at gene body with high levels of H2A.Z at TSS), H2A.Z deposition depended on both ARP6 and MBD9; however, this

loss did not cause major transcriptional changes even in *arp6-1 mbd9-3* where H2A.Z levels were nearly depleted (Supplementary Fig. 6a, b). This perhaps is not surprising since genes that typically change in expression (become up-regulated) upon H2A.Z misregulation are weakly expressed/environmentally responsive genes that contain highest levels of H2A.Z over the gene body and the TSS^{17,23–25,59,60}, most likely reflecting changes in chromatin accessibility^{23,25}. We next profiled H2A.Z changes in the significantly up- and down-regulated genes in our RNA-seq datasets (Fig. 3e). Both up- and down-regulated genes lost H2A.Z in *arp6-1* and *arp6-1 mbd9-3* mutants (Supplementary Fig. 5d). In agreement with the observed general trends, the up-regulated genes tend to belong to gene classes containing high levels of H2A.Z over the gene body (LH, MH, HH classes). More specifically, loss of H2A.Z in *mbd9-3* was observed most over genes up-regulated in *mbd9-3* ($n = 84$ and $n = 33$) and those specifically up-regulated in *arp6-1 mbd9-3* ($n = 218$) (Supplementary Fig. 5d), suggesting that MBD9-dependent H2A.Z deposition may be directly involved in repression of this subset of genes. *arp6-1* dependent up-regulated genes ($n = 252$ and $n = 500$) had minimal if any change in H2A.Z levels in *mbd9-3* (Supplementary Fig. 5d). The down-regulated genes did not tend to belong to any particular class of H2A.Z-containing genes (Fig. 3e). Except for few well-studied genes (MADS-box proteins), the down-regulated genes in the SWR1-C mutants (including MBD9) most likely reflect indirect effects related to H2A.Z loss perhaps due to misregulated transcription factors in our mutants (Supplementary Fig. 7). Altogether, these data suggest that (1) *mbd9-3* has a much weaker effect on transcription than *arp6-1*; (2) genes misregulated in the *mbd9-3* background are a subset of genes misregulated in the *arp6-1* background; (3) MBD9 and ARP6 also cooperate to control the expression of a subset of up-regulated genes; and (4) although loss of H2A.Z is observed genome-wide in *arp6-1*, and is even more pronounced in *arp6-1 mbd9-3*, genes that change in expression upon the loss of H2A.Z are generally those that contain high levels of H2A.Z at TSS and high-medium levels of H2A.Z over the gene body.

MBD9 occupies nucleosome-depleted regions near active genes. To determine the localization of MBD9 in chromatin, we performed MBD9 ChIP-seq on our complementing *pMBD9: MBD9-3xFLAG* T4 transgenic line, with wild type as a control (Supplementary Fig. 2). Using MACS2 (q value <0.01), we defined 10,348 MBD9-occupied peaks, corresponding to 5772 genes

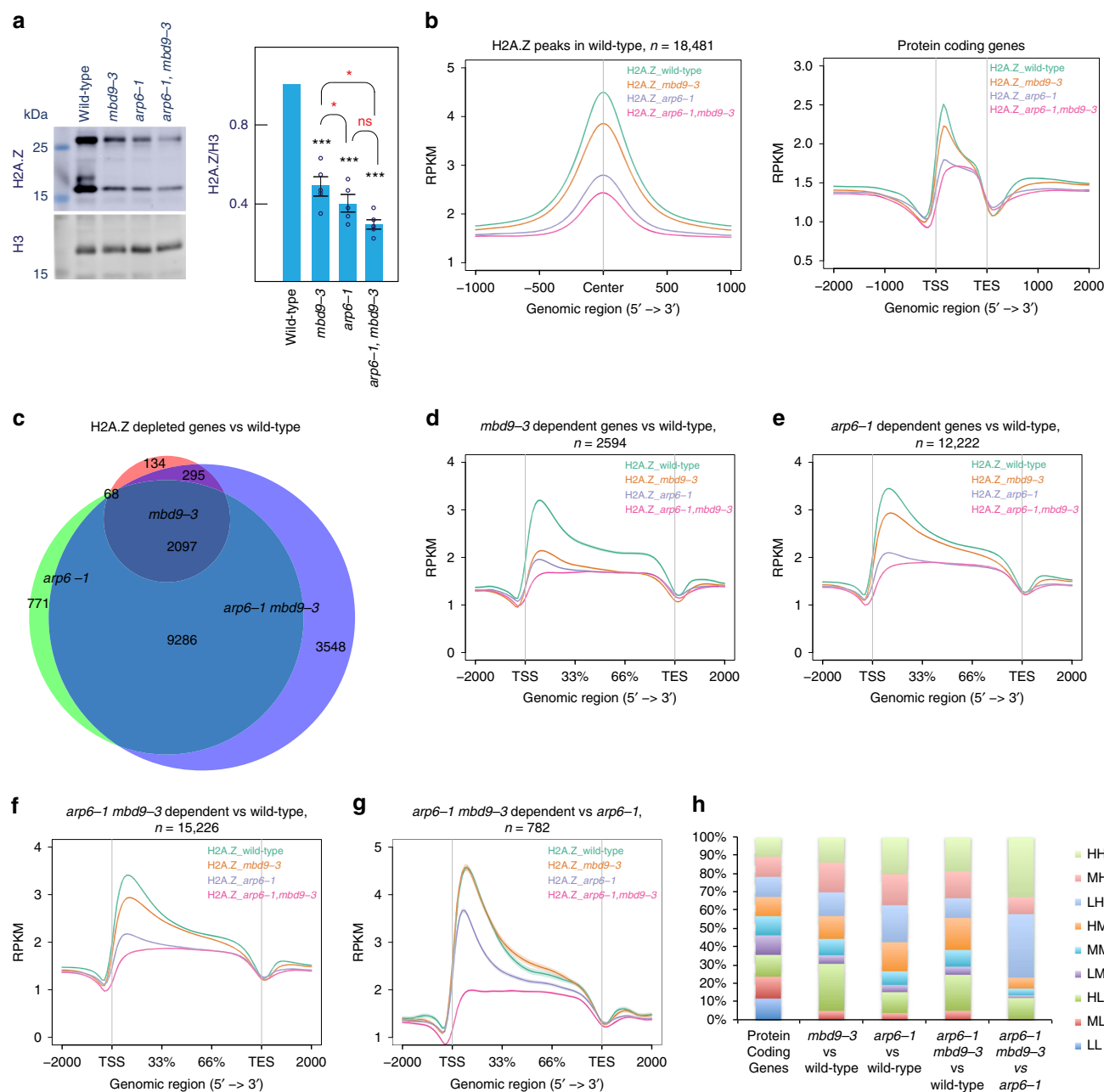
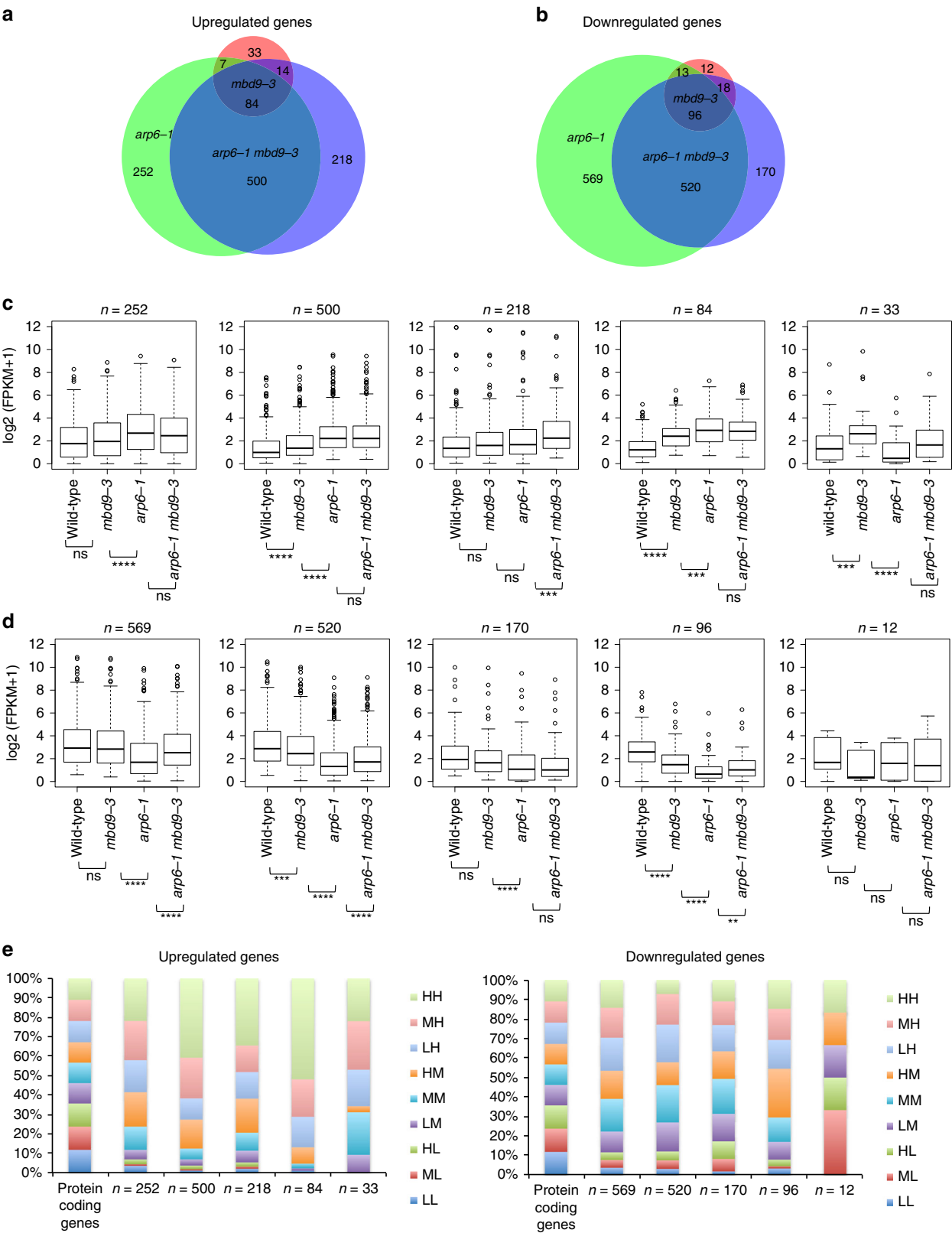


Fig. 2 Characterization of H2A.Z in wild type and mutant chromatin. **a** Western blot and quantification for H2A.Z and H3 levels in total extracts from wild type, *mbd9-3*, *arp6-1*, and *arp6-1 mbd9-3*. The upper band in the H2A.Z blot likely represents a modified form of H2A.Z. Only the lower band was used in the quantification. Average levels of three independent westerns \pm standard deviations are shown. Paired two-tailed Student's *t*-test was used to determine significance between wild type and mutants (black asterisks) or between mutants (red asterisks); ns *p* value >0.05 , **p* value ≤ 0.05 , ***p* value ≤ 0.01 , ****p* value ≤ 0.001 . **b** Distribution of normalized H2A.Z ChIP-seq signal as read count kb^{-1} million $^{-1}$ mapped reads (RPKM) from merged replicates over H2A.Z common peaks in wild type and protein-coding genes. **c** Overlap of H2A.Z-depleted genes for *mbd9-3*, *arp6-1*, and *arp6-1 mbd9-3* mutants. **d-g** Distribution of normalized H2A.Z ChIP-seq signal (RPKM) from merged replicates over H2A.Z-enriched genes for indicated mutants. **h** Intersection of H2A.Z-depleted genes from **d** to **g** with nine classes of genes characterized by their distribution of H2A.Z in wild type at TSS and gene body. Labels H—high, M—medium, L—low refer to levels of H2A.Z at TSS (first letter) and gene body (second letter). Source data for Figs. 2a and 2c are provided as Source Data file

having a peak within 1 kb upstream of the TSS (Supplementary Methods). The distribution of all MBD9 peaks showed a preference for promoter and intergenic regions (68%) compared to a control set of peaks randomly selected from the genome based on length and number (Fig. 4a). Although MBD9 contains a methyl-CpG-binding domain, it is predicted not to bind methylated DNA since it lacks key conserved residues required for mCpG binding⁶¹. Consistently, the level of methylation over MBD9 peaks in

wild-type plants was lower in all cytosine contexts than over a control set of peaks (Fig. 4b).

We plotted MBD9 peaks alongside open chromatin regions, as determined by ATAC-seq, given MBD9's clear preference for promoter regions. This revealed a significant overlap between MBD9 peaks and open chromatin regions (Fig. 4c). At these regions, the open chromatin was largely unaffected in *mbd9-3* (Fig. 4c). Metaplots of MBD9 ChIP-seq signal over



protein-coding genes revealed two major MBD9 peaks, one over nucleosome-depleted regions just upstream of the TSS and a smaller peak just 3' of the transcription end site (TES) (Fig. 4d). At the 5' end, the MBD9 peaks overlap with the ATAC-seq peaks and are just upstream of the H2A.Z peak (Fig. 4d, e).

We further investigated MBD9 occupancy in relation to H2A.Z distribution. When plotting H2A.Z over MBD9-occupied genes, we detected a loss of H2A.Z at the 5'-ends of genes in the *mbd9-3* mutant (Fig. 4f). To investigate whether the loss of H2A.Z occurs over a specific subset of genes, we ordered MBD9-occupied genes based on H2A.Z occupancy in the wild type using *k*-means

Fig. 3 RNA-seq and H2A.Z levels in wild type and mutants. **a** Overlap between significantly ($\log_2 \geq 1$, $\text{FDR} \leq 0.05$) up-regulated and **b** down-regulated genes for each mutant vs wild-type control. Boxplots of average normalized RNA-seq reads $\log_2(\text{FPKM} + 1)$ represent different classes of overlapping and non-overlapping **c** up-regulated and **d** down-regulated genes based on intersection. Center line indicates the median, upper and lower bounds represent the 75th and the 25th percentile, respectively, whiskers indicate the minimum and the maximum, and outliers are represented as circles. Unpaired two-samples Wilcoxon test was used to determine significance: ns p value > 0.05 , $*p$ value ≤ 0.05 , $**p$ value ≤ 0.01 , $***p$ value ≤ 0.001 , $****p$ value ≤ 0.0001 . **e** Intersection of up-regulated and down-regulated genes with nine classes of genes characterized by their distribution of H2A.Z in wild type at TSS and gene body. Labels H—high, M—medium, L—low refer to levels of H2A.Z at TSS (first letter) and gene body (second letter). Source data are provided as Source Data file

clustering ($n = 5$) to reflect typical patterns of H2A.Z occupancy in *Arabidopsis*¹⁷ (Fig. 4g). This analysis revealed that MBD9 occupies genes with various H2A.Z localization patterns, including genes with low H2A.Z throughout (cluster 2, Fig. 4g) and genes containing H2A.Z over gene bodies (clusters 1 and 5, Fig. 4g). However, the locations that were most sensitive to the loss of H2A.Z in the *mbd9-3* mutants were those that contain H2A.Z predominately over their 5'-ends (clusters 3 and 4, Fig. 4g, ratio plots). These regions (clusters 3 and 4) contain low levels of H3K27me3. This is in contrast to the *arp6-1* and the *arp6-1 mbd9-3* mutants, where H2A.Z loss occurred throughout all MBD9-occupied genes, with the greatest loss observed in the double mutant (Fig. 4g).

MBD9-enriched genes contain specialized chromatin features.

To determine if specific chromatin features mark the regions that are enriched with MBD9, we analyzed ATAC-seq data from wild-type plants and observed that MBD9-occupied genes tended to have more open chromatin than either an equivalent set of genes with similar expression levels, or all protein-coding genes (Fig. 5a, b). We also investigated preferences for histone modifications using previously published and generated data^{62–64} from equivalent tissues and stages of development (Supplementary Note). MBD9-occupied genes contained higher levels of H3K4me3 when compared to all protein-coding genes and the H3K4me3 signal was broader when compared to a control set of genes (Fig. 5c). A similar relative enrichment was also true for histone acetylation levels (Fig. 5c), whereas MBD9-occupied genes were depleted of H3K27me3 when compared to gene averages (Fig. 5c). This general trend was also true for regions depleted of H2A.Z in *mbd9-3*, as depicted in the heatmap ordered by expression level at all protein-coding genes (Supplementary Fig. 8). Regions that lost H2A.Z most in *mbd9-3* tended to occur predominantly at the 5'-ends of genes. These regions also contained high levels of activating histone modifications (H3K4me3, H3Ac) and low levels of H3K27me3, and coincided with MBD9-occupied peaks and open chromatin. In agreement, a related study also identified an enrichment of histone acetylation marks at MBD9-dependent H2A.Z sites⁵⁴.

Altogether, these results suggest that MBD9 preferentially localizes to the open chromatin regions of actively transcribing genes, which contain high levels of H3K4me3 and histone acetylation and are different from genes controlled by the Polycomb Group Complex.

Discussion

H2A.Z has been implicated in a wide variety of functions, including transcription, meiosis, and DNA damage⁵². How it is specifically targeted to the locations where these events occur is poorly understood. In this study we have characterized the interacting partners of *Arabidopsis* ARP6, a homolog of Arp6 found in the yeast SWR1-C involved in H2A.Z deposition. We identified nine *Arabidopsis* proteins that are homologous to subunits common to the yeast (SWR1) and mammalian (SRCAP)

complexes, ARP6, PIE1, RIN1, RIN2, ARP4, SWC4, SWC2, YAF9A, and SEF. We further identified several additional ARP6-interacting partners, TRA1A, TRA1B, MBD9, and four members of the Alfin1-like family (AL4, AL5, AL6, and AL7). These Alfin1-like-containing proteins recognize H3K4me3 histones⁵⁷, suggesting that they play a role in recruiting the SWR1 complex to H3K4me3 regions. The ARP6-interacting partners identified in our study are in agreement with a related study involving ARP6-TAP purification followed by mass spectrometry⁵⁴. However, there were a few differences. Specifically, we did not enrich for H2A.Z or ACT1 in our mass spec data, perhaps reflecting different methods of isolation, while we did identify TRA1A and AL4 as ARP6-interacting partners that were not reported by Sijacic et al.⁵⁴.

We focused on characterizing the interaction between ARP6 and MBD9. We identified interacting partners for MBD9 and showed that it interacted with most components of the SWR1 complex, including PIE1, RIN1, ARP4, RIN2, SWC2, ARP6, SWC4, YAF9A, and SEF. MBD9 also interacted with TRA1A and TRA1B, further implicating histone acetylation in H2A.Z deposition. Additionally, we detected high enrichment of the ISWI chromatin remodeling complex in our MBD9 IP, which was not seen in the ARP6 IP—mass spec. The ISWI remodeling complex interacts with other chromatin remodelers⁶⁵, MADS proteins⁶⁶, and DTT-containing proteins⁶⁷. MBD9 was among the reported interacting partners of CHR17, independently validating our results⁶⁵. However, only two other SWR1 complex components (ARP4 and RIN1) were detected in the same CHR17 IP—mass spec study. Since we did not detect preferential enrichment between CHR11/17 and ARP6 in our data, this suggests that MBD9 interacts with the two complexes separately. Our analysis of the genetic interactions between *mbd9-3* and *arp6-1* suggests that, despite the more severe developmental phenotype of the double mutant, ARP6 is epistatic to MBD9 regarding flowering time. These two observations are in agreement since flowering time is controlled by a particular set of genes, whereas H2A.Z deposition is globally affected in our mutants. The stronger developmental phenotype of the double mutant could have two plausible explanations: (1) multiple pathways are involved or (2) since the double mutant closely resembles *pie1-2* (a mutation affecting the catalytic subunit of the SWR1 complex), the phenotype results from MBD9 and ARP6 being part of the SWR1 complex, where the complex may be partly functional without one of the components but not without both. Future work will discriminate between these possibilities. Our genomic observations, H2A.Z ChIP-seq data, and transcriptome analysis revealed that MBD9 and ARP6 share many common targets, but the *mbd9-3* mutant shows a weaker phenotype than *arp6-1*. We observed that MBD9 is required for the deposition of H2A.Z at a subset of *arp6-1* dependent loci, similar to what was reported by Sijacic et al.⁵⁴. We also identified a subset of genes that require both ARP6 and MBD9 for both their expression and for H2A.Z deposition, suggesting the two proteins act redundantly in some cases. Additionally, we determined the genome-wide occupancy of MBD9 and showed that it

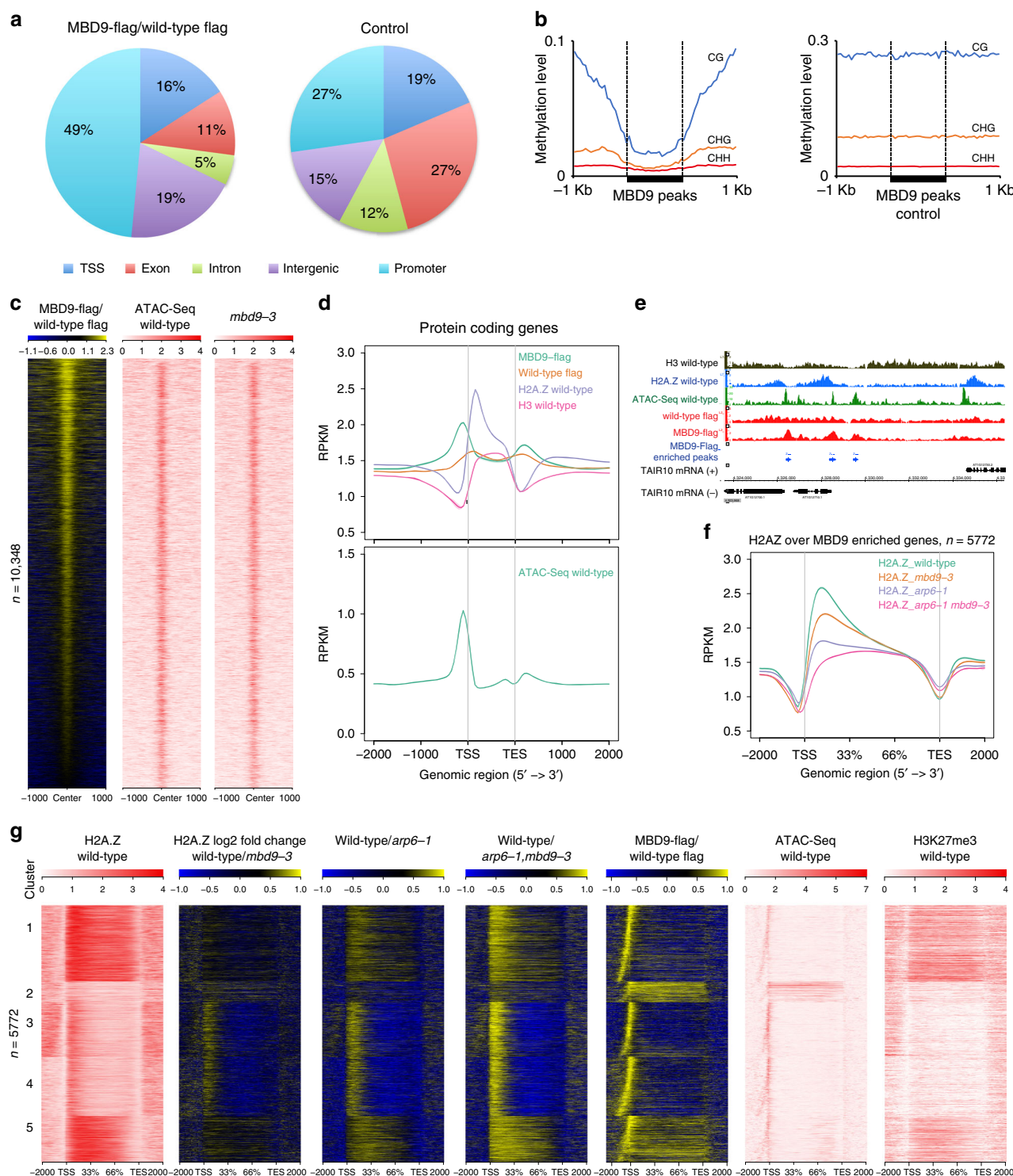


Fig. 4 Characterization of MBD9 chromatin binding. **a** Genomic distribution of MBD9-enriched peaks vs wild type (mac2 peak caller, *q* value < 0.01). **b** Average distribution of DNA methylation levels in CG, CHG, and CHH contexts in wild type over MBD9-occupied peaks and MBD9 control peaks. **c** Heatmap of normalized MBD9 signal (\log_2 RPKM) over wild-type control and normalized ATAC-seq signal (RPKM) from merged replicates in wild type and *mbd9-3* mutant over MBD9-occupied peaks. **d** Upper: Distribution of normalized signal (RPKM) for MBD9-3xFlag ChIP-seq, wild-type Flag ChIP-seq control, H2A.Z, and H3 in wild type over protein-coding genes. Lower: Distribution of normalized signal (RPKM) for ATAC-seq in wild type over protein-coding genes. **e** Snapshot representing normalized read counts (RPKM) for MBD9-3xFlag ChIP-seq, wild-type Flag ChIP-seq control, ATAC-seq, H2A.Z, and H3. Signal for ATAC-seq, H2A.Z, and H3 is a merge of two biological replicates. **f** Distribution of normalized H2A.Z ChIP-seq signal (RPKM) from merged replicates in wild type, *mbd9-3*, *arp6-1*, and *arp6-1 mbd9-3* over MBD9-occupied genes. **g** Heatmap ordered based on *k*-means clustering of H2A.Z ChIP-seq signal in wild type (cluster *n* = 5) at MBD9-occupied genes. Shown are corresponding H2A.Z ratio plots for wild type over *mbd9-3*, *arp6-1*, and *arp6-1 mbd9-3* mutants and MBD9-3X Flag ChIP-seq over wild-type flag control in \log_2 RPKM, ATAC-seq in wild type in RPKM, and H3K27me3 levels in wild type in RPKM. Source data are provided as Source Data file

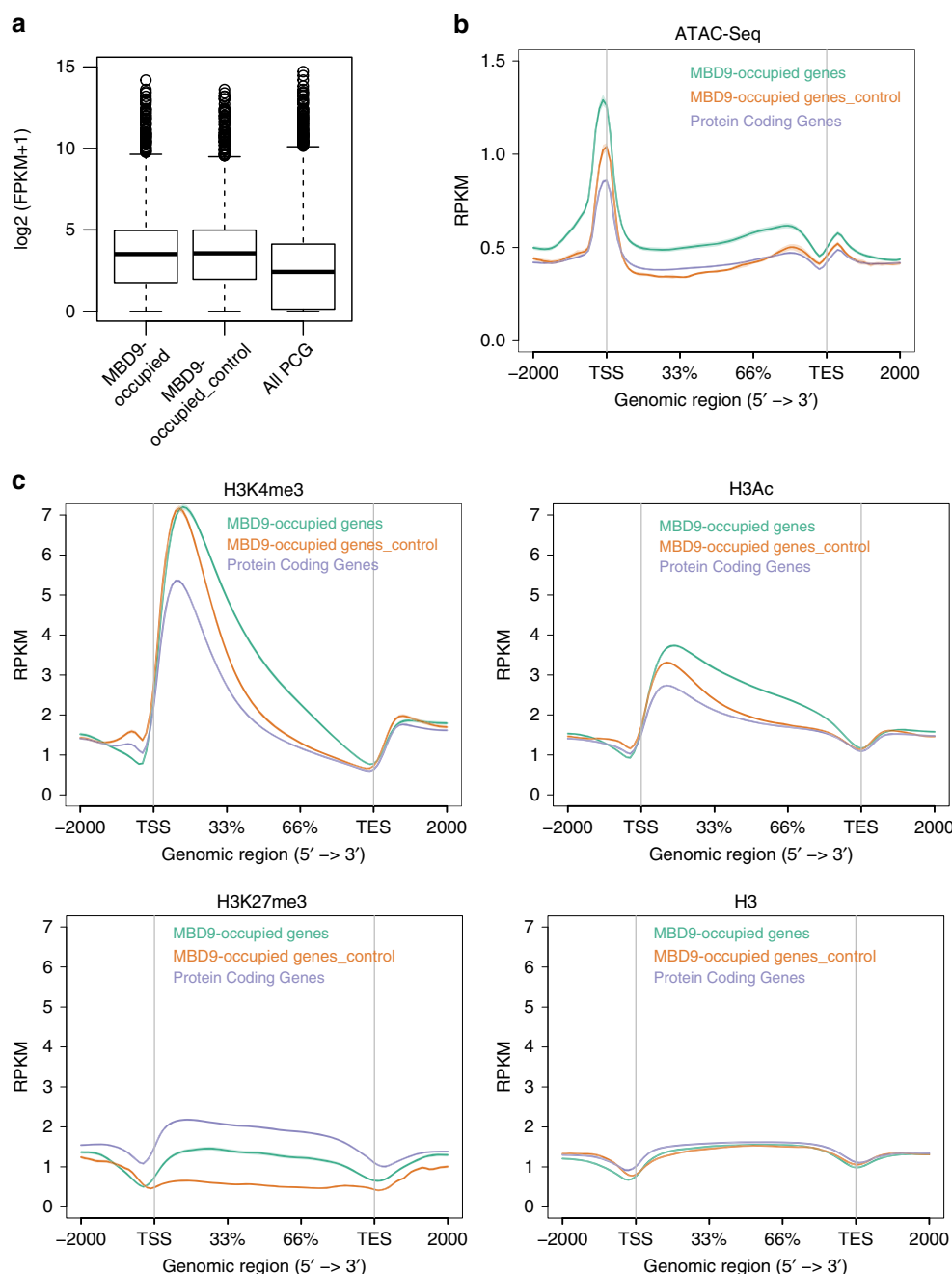


Fig. 5 Chromatin features at MBD9-occupied genes. **a** Boxplots of average expression levels $\log_2(\text{FPKM} + 1)$ from RNA-seq in wild type for MBD9-occupied genes, MBD9 control genes, and protein-coding genes. Center line indicates the median, upper and lower bounds represent the 75th and the 25th percentile, respectively, whiskers indicate the minimum and the maximum, and outliers are represented as circles. **b** Distribution of normalized ATAC-seq levels (RPKM) over MBD9-occupied genes, MBD9 control genes, and protein-coding genes. **c** Distribution of normalized levels (RPKM) for H3K4me3, H3Ac, H3K27me3, and H3 ChIP-seq in MBD9-occupied genes, MBD9 control genes, and protein-coding genes

preferentially localized to the open chromatin regions of promoters and the transcription termination sites of active genes that have high levels of activating histone modifications (H3K4me3 and histone acetylation) and did not localize to genes repressed by the Polycomb Group Complex. These data suggest that the MBD9-containing SWR1 complex promotes H2A.Z deposition at the 5' ends of highly expressed genes.

Regarding the interaction of MBD9 with the SWR1 complex, three possibilities exist based on our genetic and genomic observations: (1) MBD9 is always a member of the SWR1 complex but not always required, (2) MBD9 is part of a subset of all SWR1 complexes in *Arabidopsis*, and (3) MBD9 only transiently interacts

with the SWR1 complex. Based on size exclusion chromatography of ARP6-containing SWR1 complex in the *mbd9* mutant, Sijacic et al.⁵⁴ concluded that MBD9 is not a core subunit of the *Arabidopsis* SWR1 complex. However, as noted by the authors, this does not exclude the possibility that MBD9 is part of a small subset of all SWR1 complexes in *Arabidopsis*⁵⁴. Given that we detected most components of the SWR1 complex in our MBD9 IP-mass spec, our genetic and genomic data best fit the model that MBD9 is part of a subset of the SWR1-containing complexes.

Surprisingly, although we detected many genes that lost H2A.Z in the *mbd9-3* mutant, this loss did not result in major transcriptional changes. This may be because the loss of H2A.Z in the

mbd9-3 mutant occurs over genes with low H2A.Z over gene bodies and several studies suggest that genes changing most upon loss of H2A.Z are the ones bearing H2A.Z over the gene body^{17,23,24}. One plausible explanation for the lack of transcriptional response at these regions in the *mbd9-3* mutant is redundancy. It is possible that redundant mechanisms are present at housekeeping genes to maintain their high expression and losing H2A.Z is not enough to perturb their activity. In support, H2A.Z is proposed to have redundant roles with chromatin remodeling complexes in yeast⁶⁸. Interestingly, we identify components of the ISWI chromatin remodeling family as interacting partners of MBD9 in our IP. Additionally, CHR11/17 mutants have defects in flowering time and decreased levels of *FLC* expression⁶⁹. Perhaps in addition to promoting H2A.Z deposition, MBD9 promotes low nucleosome occupancy at genes containing H2A.Z at +1 by interacting with chromatin remodelers to maintain these loci in a transcriptionally permissive state. In support, a recent study of FORGETTER1, a protein involved in heat-shock memory response, was found to interact with chromatin remodelers including CHR11/17 to maintain low nucleosome occupancy of genes in non-inductive conditions⁶⁵. In *Arabidopsis*, the ISWI remodeling complex is required for the regular spacing of nucleosomes downstream of the +1 border nucleosome⁷⁰. Interestingly, many highly expressed genes in the CHR11/17 mutant have defects in nucleosome positioning, yet their transcription is unaffected⁷⁰. This finding supports our hypothesis that redundant mechanisms maintain high expression of housekeeping genes. Higher order mutants between the SWR1 complex and chromatin remodelers are required to test this hypothesis.

In yeast, the SWR1 complex preferentially binds to nucleosome-depleted regions^{42,43}. Consistent with the role of MBD9 in the SWR1 complex, we found that MBD9 also localizes to nucleosome-depleted regions, in close proximity to H2A.Z deposited at the 5'-ends of gene bodies. These regions are devoid of DNA methylation, consistent with the prediction that the methyl-binding domain of MBD9 does not recognize methylated sequences⁶¹.

The genes bearing MBD9 also contain high levels of histone acetylation, consistent with the observation that histone acetylation in yeast promotes H2A.Z deposition. We also observed enrichment of three of the four common NuA4 histone acetylation complex subunits, SWC4, YAF9, and ARP4, in our IP-mass spec. We also identified two homologs of the yeast Tra1 proteins, TRA1A and TRA1B, in both ARP6 and MBD9 IPs. Tra1 is a component of the yeast NuA4 complex⁵⁰. In *Arabidopsis*, TRA1B interacts with SWC4, a component of the predicted NuA4 complex⁷¹, and both TRA1A and TRA1B are components of the *Arabidopsis* SAGA acetyltransferase complex⁷². This suggests that various acetyltransferase complexes may be promoting H2A.Z deposition via histone acetylation. Since we did not detect the NuA4 scaffold or the catalytic subunit in our IP, it is unlikely that the ARP6-containing SWR1 complex represents a fusion of the *Arabidopsis* SWR1 and NuA4 complexes, similar to the mammalian TIP60 complex; rather, the TRA1A and TRA1B subunits may function to bridge the acetyltransferases with the SWR1 complex.

In summary, our study identified components of the SWR1 complex in *Arabidopsis* and shed light on the role of MBD9 in promoting H2A.Z deposition at a subset of highly expressed genes. Further work addressing the function of the H2A.Z histone variant should reveal the nature of its dependency on factors such as histone acetyltransferase and chromatin remodeling complexes for carrying out its varied functions across the genome.

Methods

Plant materials. All *Arabidopsis* plants used in this study were of the Col-0 ecotype and were grown at 22 °C under long-day conditions (16 h light, 8 h dark). For the

short-day flowering time experiment, plants were grown at 22 °C (16 h dark, 8 h light). The following *Arabidopsis* mutant lines were used: *mbd9-3* (SALK_039302), *arp6-1* (Sail_599_G03), and *pie1-2* (SALK_003776C).

Quantitative real time PCR. Total RNA was prepared from whole seedlings (14 DAG) using the RNA Prep Pure Plant Kit (Tiangen Biotech, Beijing, China). Two micrograms of RNA was used for the preparation of cDNA using PrimeScript Reagent Kit with gDNA eraser (Takara, Japan). Signal detection, quantification, and normalization were done using Quant Studio 6 proprietary Software (Life Technologies, USA).

Co-immunoprecipitation. An anti-MBD9 polyclonal antibody was raised in rabbits using the 1941–2176 aa MBD9 peptide as an antigen. The antibody was coupled to magnetic beads using the Dynabeads antibody coupling kit (Invitrogen, USA) following the manufacturer's recommendations; 7 µL of 3.12 mg mL⁻¹ were used per sample. Approximately 2 g of floral tissue was ground in liquid nitrogen, 10 mL IP buffer (50 mM Tris pH 7.6, 150 mM NaCl, 5 mM MgCl₂, 10% glycerol, 0.1% NP-40, 0.5 mM DTT, 1 µg mL⁻¹ pepstatin, 1 mM PMSF, 1 protease inhibitor cocktail tablet (Roche, 14696200)) was added, the mix was incubated on ice for 20 min, and spun at 4000g for 10 min at 4 °C. The supernatant was filtered through a double layer of Miracloth. Anti-MBD9 antibody coupled to magnetic beads was added and incubated for 2 h at 4 °C with gentle rotation. Beads were washed six times with IP buffer, 5 min each wash at 4 °C with rotation, and then boiled. Western blotting and detection were performed with anti-Myc 9E10 mouse monoclonal antibody (Thermo Fisher Scientific, MA1-980) with 1:1000 dilution.

RNA-seq and analysis. Total RNA was extracted from 13 DAG shoots grown on 1% MS supplemented with 1% sucrose under long-day conditions. Four replicates, grown on separate plates, were collected for each genotype. RNA was extracted using the Direct-zol RNA Miniprep kit (Zymo). For RNA-seq, 1 µg of total RNA was used to prepare libraries using the TruSeq Stranded mRNA-Seq kit (Illumina). Reads were aligned to TAIR10 using Tophat by allowing up to two mismatches and mapping only to one location. FPKM values and differential gene expression were analyzed using Cufflinks with default settings. GO term enrichment was determined using AgriGO.

Epitope-tagged transgenic ARP6 and MBD9 lines. Full-length genomic DNA fragments containing ~1 kb (MBD9) or ~1.5 kb (ARP6) of promoter sequence, together with genomic gene sequences up to the annotated/major stop codon of MBD9 and ARP6 were amplified using PCR (primers are listed in Supplementary Table 1). The PCR product was cloned into the pENTR/D vector (Invitrogen) and delivered into a modified pEG containing 3X FLAG and 9X MYC tags using the LR reaction kit (Invitrogen). The pEG destination vectors were transformed into *Agrobacterium* strain AGL0, followed by transformation using the floral dip method.

Affinity purification and mass spectrometry. Approximately 10 g of flowers from transgenic lines expressing T3 ARP6-3xFLAG or T4 MBD9-3xFLAG and from Col-0 plants as negative controls were ground to a fine powder using a RETCH homogenizer (3 min @ 30 Hz min⁻¹) and suspended in 30 mL of IP buffer. Tissue was further dounce homogenized until lump-free, then centrifuged for 20 min at 4000g and 4 °C. The lysate was filtered through two layers of Miracloth. Supernatant was incubated with 200 µL anti-FLAG M2 magnetic beads (M8823, Sigma), at 4 °C for 2 h. The bead-bound complex was washed once with 10 mL IP buffer, then four times (5 min rotating at 4 °C with 1.5 mL IP buffer), followed by a final wash with IP buffer without NP-40. The FLAG-IP was eluted twice with 300 µL 250 µg mL⁻¹ 3X FLAG peptides (Sigma, F4799) in TBS (50 mM Tris-Cl, pH 7.5, 150 mM NaCl), mixing for 15 min at 4 °C. The eluted protein complexes were precipitated by trichloroacetic acid and subjected to mass spectrometric analyses. In the case of ARP6-9xMyc and MBD9-9xMyc, monoclonal 9E10 coupled to magnetic beads was used (88842, Pierce). The bead-bound complexes were washed six times with 1 mL of IP buffer. For each wash, the beads were rotated at 4 °C for 5 min. For ARP6-9xMyc, proteins were released from the Streptavidin beads by 3C cleavage overnight at 5 °C. 3C-GST was removed by incubation with GST couple magnetic beads (Pierce, USA). For MBD9-9xMyc, proteins were eluted twice with 100 µL 8 M Urea in 50 mM Tris pH 8.5, mixing for 15 min at 37 °C. The supernatant was TCA precipitated.

Genome-wide ChIP sequencing and library generation. For histone modification ChIPs, about 0.5 g of shoots were collected from 13 DAG seedlings grown on 1% MS plates supplemented with 1% sucrose under long-day conditions. Samples were crosslinked in vitro, sheared using Bioruptor Plus (Diagenode). Libraries were generated with NuGEN Ovation Ultra Low System V2 kit, according to the manufacturer's instructions, and were sequenced on an Illumina HiSeq 4000 instrument. H2A.Z ChIP assays were performed using polyclonal antibodies specific to *Arabidopsis* H2A.Zs HTA11 and HTA9. The antibodies were produced in rabbits and further purified using the peptides described in Deal et al.⁵⁷. For each ChIP we used 4 µL of 3.34 mg mL⁻¹. Abcam1791 (Abcam) antibody was used for

H3 ChIP assays (10 μ L of 0.5 mg mL⁻¹) and active motif 39140 (Active Motif) was used for pan-acetyl H3 ChIP assays (5 μ L of 1 mg mL⁻¹).

For MBD9, about 5 g of 13 DAG T4 MBD9-3XFLAG and Col-0 seedlings grown on 1% MS were fixed *in vivo* using vacuum infiltration as follows. Protein-protein crosslinking was performed first using 1.5 mM EGS in 1× phosphate-buffered saline (PBS) for 10 min followed by three washes with PBS. Next, tissue was fixed with 1% formaldehyde in 1× PBS for 20 min. Crosslinking was stopped with 0.125 M glycine in 1× PBS and the seedlings were vacuum infiltrated for 5 min. Tissue was patted dry and frozen at -80 °C. Tissue was homogenized to a fine powder using a RETCH homogenizer (2 min @ 30 Hz min⁻¹) and resuspended with Nuclear Isolation Buffer (50 mM Hepes, 1 M Sucrose, 5 mM KCl, 5 mM MgCl₂, 0.6% Triton X-100, 0.4 mM PMSF, 5 mM Benzamide, 1× protease inhibitor cocktail tablet (Roche, 14696200). Lysate was filtered through one layer of Miracloth and centrifuged for 20 min at 2880g and 4 °C. The pellet was resuspended with 1 mL Extraction buffer 2 (0.25 M sucrose, 10 mM Tris-HCl pH 8, 10 mM MgCl₂, 1% Triton X-100, 5 mM BME, 0.1 mM PMSF, 5 mM Benzamide, and 1× protease inhibitor cocktail tablet (Roche, 14696200)), followed by centrifugation for 10 min at 12,000g and 4 °C. The pellet was then resuspended in 500 μ L Extraction buffer 3 (1.7 M sucrose, 10 mM Tris-HCl pH 8, 2 mM MgCl₂, 0.15% Triton X-100, 5 mM BME, 0.1 mM PMSF, 5 mM Benzamide, 1× protease inhibitor cocktail tablet (Roche, 14696200)), layered over 500 μ L extraction buffer 3 and centrifuged for 1 h at 12,000g and 4 °C. The pellet was lysed with 400 μ L Nuclei Lysis Buffer on ice (50 mM Tris pH 8, 10 mM EDTA, 1% SDS, 0.1 mM PMSF, 5 mM Benzamide, 1× protease inhibitor cocktail tablet (Roche, 14696200)). To lysed nuclei, 1.7 mL of ChIP Dilution Buffer (1.1% Triton X-100, 1.2 mM EDTA, 16.7 mM Tris pH 8, 167 mM NaCl, 0.1 mM PMSF, 5 mM Benzamide, 1× protease inhibitor cocktail tablet (Roche, 14696200) was added and DNA was sheared on a Bioruptor Plus (Diagenode) (30 s ON/30 s OFF, Max power, 17 min at 4 °C). Sheared chromatin was centrifuged twice at max speed for 10 min at 4 °C. The supernatant was further diluted with ChIP dilution buffer up to 4 mL. One hundred microliters of sample were saved as input and the rest was split into 2 mL DNA LoBind tubes (Eppendorf, D1579630) and 10 μ L of 1 mg mL⁻¹ anti-Flag antibody was added (F1804; Sigma-Aldrich). After incubation overnight with rotation at 4 °C, 50 μ L Dynabeads (equal mix of Protein A and G; Invitrogen 10004D/10002D) was added to chromatin and incubated for an additional 2 h. The magnetic beads were washed with 1 mL of the following buffers for 5 min rotating at 4 °C: 2× with low salt buffer (150 mM NaCl, 0.2% SDS, 0.5% Triton X-100, 2 mM EDTA, 20 mM Tris pH 8), 1× high salt buffer (200 mM NaCl, 0.2% SDS, 0.5% Triton X-100, 2 mM EDTA, 20 mM Tris pH 8), 1× LiCl Wash Buffer (250 mM LiCl, 1% Igepal, 1% sodium deoxycholate, 1 mM EDTA, 10 mM Tris pH 8), and 1× with TE buffer (10 mM Tris pH 8, 1 mM EDTA). The immunocomplex was eluted from the beads twice with 250 μ L elution buffer (1% SDS, 10 mM EDTA, 0.1 M NaHCO₃), incubating for 20 min with shaking at 65 °C. Four hundred microliters of elution buffer was added to the input samples. A total of 20 μ L 5 M NaCl was added to each tube; the crosslink was reversed by incubation at 65 °C overnight. Residual protein was degraded with 20 μ L Prot K in 10 mM EDTA and 40 mM Tris pH 8 at 45 °C for 1 h followed by phenol/chloroform/isoamyl alcohol extraction and ethanol precipitation. The pellet was washed with 70% EtOH and resuspended in 50 μ L molecular grade water. Libraries were prepared using the NuGEN Ovation Ultra Low System V2 kit, according to the manufacturer's instructions, and were sequenced on an Illumina HiSeq 4000 instrument.

ChIP-seq analysis. ChIP-seq fastq reads were aligned to the TAIR10 reference genome with Bowtie using default settings and allowing only uniquely mapping reads. Duplicated reads were removed using SAMtools. IGB genome browser was used to visualize the data and to generate snapshots. Normalized read coverage tracks were generated using the USeq package Sam2Useq application. ChIP-seq peaks in wild type and mutants were called by callpeak function in MACS2 (v2.1.1). ChIP-seq data metaplots and *k*-means clustering were generated by NGSPlot (v4.02.48). Enriched motifs in peak sets were identified using HOMER findMotifsGenome. Annotation of peak locations were carried out using the HOMER annotatepeaks function. GO term enrichment was determined using AgriGO.

ATAC-seq. Inflorescence tissues were collected for nuclei extraction as follows. About 5 g of inflorescence tissue was collected and immediately transferred into ice-cold grinding buffer (300 mM sucrose, 20 mM Tris pH 8, 5 mM MgCl₂, 5 mM KCl, 0.2% Triton X-100, 5 mM β -mercaptoethanol, 35% glycerol). The samples were ground with an Omni International General Laboratory Homogenizer at 4 °C and then filtered through a two-layer Miracloth and a 40- μ m nylon mesh Cell Strainer (Fisher). Samples were spin filtered for 10 min at 3000g, the supernatant discarded, and the pellet resuspended with 25 mL of grinding buffer using a Dounce homogenizer. The wash step was repeated once and the nuclei resuspended in 0.5 mL of freezing buffer (50 mM Tris pH 8, 5 mM MgCl₂, 20% glycerol, 5 mM β -mercaptoethanol). Nuclei were subjected to transposition reaction with Tn5 (Illumina, cat. no. FC-121-1030)⁷³. For transposition reaction, 25 μ L of 2× DMF (66 mM Tris-acetate (pH = 7.8), 132 K-Acetate, 20 mM Mg-Acetate, 32% DMF) was mixed with 2.5 μ L Tn5 and 22.5 μ L nuclei suspension and incubated at 37 °C for 30 min⁷³. Transposed DNA fragments were purified with ChIP DNA Clean & Concentrator Kit (Zymo, cat. no. D5205)⁷³. Libraries were generated using Phusion High-Fidelity DNA Polymerase (NEB, cat. no. M0530S) as follows, 12.5 μ L

2× Phusion, 1.25 μ L 10 mM Ad1 primer, 1.25 μ L 10 mM Ad2 primer, 4 μ L ddH₂O and 6 μ L purified transposed DNA fragments were mixed and subjected to 12 cycles of PCR amplification (72 °C for 5 min, 12 cycles of 98 °C for 3 min, 98 °C for 45 s, 63 °C for 30 s, and 72 °C for 1 min)⁷³. Libraries were sequenced on an Illumina HiSeq 2000 instrument. ATAC-seq read adaptors were removed with trim_galore and then mapped to the *Arabidopsis thaliana* reference genome TAIR10 using Bowtie (-X 2000 -m 1). Chloroplast and mitochondrial DNA aligned reads were filtered out and duplicate reads were removed using SAMtools.

Reporting Summary. Further information on research design is available in the Nature Research Reporting Summary linked to this article.

Data availability

Data supporting the findings of this work are available within the paper and its Supplementary Information files. A reporting summary for this Article is available as a Supplementary Information file. The datasets generated and analyzed during the current study are available from the corresponding author upon request. The source data underlying Figs. 1a, 1c, 1d, 2a, 2c, 3, and 4, Supplementary Figs. 1, 2, and 6, and Tables 1, 2 are provided as a Source Data file. All high-throughput sequencing data generated in this study is accessible at NCBI's Gene Expression Omnibus (GEO) via GEO Series accession number [GSE123263](https://www.ncbi.nlm.nih.gov/geo/query/acc.cgi?acc=GSE123263).

Received: 5 December 2018 Accepted: 5 July 2019

Published online: 26 July 2019

References

- Luger, K., Rechsteiner, T. J., Flaus, A. J., Wayne, M. M. & Richmond, T. J. Characterization of nucleosome core particles containing histone proteins made in bacteria. *J. Mol. Biol.* **272**, 301–311 (1997).
- Clapier, C. R., Iwasa, J., Cairns, B. R. & Peterson, C. L. Mechanisms of action and regulation of ATP-dependent chromatin-remodelling complexes. *Nat. Rev. Mol. Cell Biol.* **18**, 407–422 (2017).
- Clapier, C. R. & Cairns, B. R. The biology of chromatin remodeling complexes. *Annu. Rev. Biochem.* **78**, 273–304 (2009).
- van Daal, A., White, E. M., Elgin, S. C. & Gorovsky, M. A. Conservation of intron position indicates separation of major and variant H2As is an early event in the evolution of eukaryotes. *J. Mol. Evol.* **30**, 449–455 (1990).
- Thatcher, T. H. & Gorovsky, M. A. Phylogenetic analysis of the core histones H2A, H2B, H3, and H4. *Nucleic Acids Res.* **22**, 174–179 (1994).
- Talbert, P. B. & Henikoff, S. Histone variants-ancient wrap artists of the epigenome. *Nat. Rev. Mol. Cell Biol.* **11**, 264–275 (2010).
- Zilberman, D., Coleman-Derr, D., Ballinger, T. & Henikoff, S. Histone H2A.Z and DNA methylation are mutually antagonistic chromatin marks. *Nature* **456**, 125–129 (2008).
- Raisner, R. M. et al. Histone variant H2A.Z marks the 5' ends of both active and inactive genes in euchromatin. *Cell* **123**, 233–248 (2005).
- Zhang, H., Roberts, D. N. & Cairns, B. R. Genome-wide dynamics of Htz1, a histone H2A variant that poises repressed/basal promoters for activation through histone loss. *Cell* **123**, 219–231 (2005).
- Mavrich, T. N. et al. Nucleosome organization in the *Drosophila* genome. *Nature* **453**, 358–362 (2008).
- Millar, C. B., Xu, F., Zhang, K. & Grunstein, M. Acetylation of H2AZ Lys 14 is associated with genome-wide gene activity in yeast. *Genes Dev.* **20**, 711–722 (2006).
- Barski, A. et al. High-resolution profiling of histone methylations in the human genome. *Cell* **129**, 823–837 (2007).
- Hardy, S. et al. The euchromatic and heterochromatic landscapes are shaped by antagonizing effects of transcription on H2A.Z deposition. *PLoS Genet.* **5**, e1000687 (2009).
- Guillemette, B. et al. Variant histone H2A.Z is globally localized to the promoters of inactive yeast genes and regulates nucleosome positioning. *PLoS Biol.* **3**, e384 (2005).
- Hu, G. et al. H2A.Z facilitates access of active and repressive complexes to chromatin in embryonic stem cell self-renewal and differentiation. *Cell Stem Cell* **12**, 180–192 (2013).
- Murphy, P. J., Wu, S. F., James, C. R., Wike, C. L. & Cairns, B. R. Placeholder nucleosomes underlie germline-to-embryo DNA methylation reprogramming. *Cell* **172**, 993–1006, e1013 (2018).
- Coleman-Derr, D. & Zilberman, D. Deposition of histone variant H2A.Z within gene bodies regulates responsive genes. *PLoS Genet.* **8**, e1002988 (2012).
- Bewick, A. J. et al. On the origin and evolutionary consequences of gene body DNA methylation. *Proc. Natl Acad. Sci. USA* **113**, 9111–9116 (2016).
- Zemach, A., McDaniel, I. E., Silva, P. & Zilberman, D. Genome-wide evolutionary analysis of eukaryotic DNA methylation. *Science* **328**, 916–919 (2010).

20. Edwards, J. R. et al. Chromatin and sequence features that define the fine and gross structure of genomic methylation patterns. *Genome Res.* **20**, 972–980 (2010).
21. Conerly, M. L. et al. Changes in H2A.Z occupancy and DNA methylation during B-cell lymphomagenesis. *Genome Res.* **20**, 1383–1390 (2010).
22. Luo, C. & Lam, E. ANCORP: a high-resolution approach that generates distinct chromatin state models from multiple genome-wide datasets. *Plant J.* **63**, 339–351 (2010).
23. Dai, X. et al. H2A.Z represses gene expression by modulating promoter nucleosome structure and enhancer histone modifications in Arabidopsis. *Mol. Plant* **10**, 1274–1292 (2017).
24. Sura, W. et al. Dual role of the histone variant H2A.Z in transcriptional regulation of stress-response genes. *Plant Cell* **29**, 791–807 (2017).
25. Kumar, S. V. & Wigge, P. A. H2A.Z-containing nucleosomes mediate the thermosensory response in Arabidopsis. *Cell* **140**, 136–147 (2010).
26. Carter, B. et al. The chromatin remodelers PKL and PIE1 act in an epigenetic pathway that determines H3K27me3 homeostasis in Arabidopsis. *Plant Cell* **30**, 1337–1352 (2018).
27. Mizuguchi, G. et al. ATP-driven exchange of histone H2AZ variant catalyzed by SWR1 chromatin remodeling complex. *Science* **303**, 343–348 (2004).
28. Krogan, N. J. et al. Regulation of chromosome stability by the histone H2A variant Htz1, the Swr1 chromatin remodeling complex, and the histone acetyltransferase NuA4. *Proc. Natl Acad. Sci. USA* **101**, 13513–13518 (2004).
29. Kobor, M. S. et al. A protein complex containing the conserved Swi2/Snf2-related ATPase Swr1p deposits histone variant H2A.Z into euchromatin. *PLoS Biol.* **2**, E131 (2004).
30. Nguyen, V. Q. et al. Molecular architecture of the ATP-dependent chromatin-remodeling complex SWR1. *Cell* **154**, 1220–1231 (2013).
31. Cai, Y. et al. The mammalian YL1 protein is a shared subunit of the TRRAP/TIP60 histone acetyltransferase and SRCAP complexes. *J. Biol. Chem.* **280**, 13665–13670 (2005).
32. Ruhl, D. D. et al. Purification of a human SRCAP complex that remodels chromatin by incorporating the histone variant H2A.Z into nucleosomes. *Biochemistry* **45**, 5671–5677 (2006).
33. Wong, M. M., Cox, L. K. & Chrivia, J. C. The chromatin remodeling protein, SRCAP, is critical for deposition of the histone variant H2A.Z at promoters. *J. Biol. Chem.* **282**, 26132–26139 (2007).
34. Verbsky, M. L. & Richards, E. J. Chromatin remodeling in plants. *Curr. Opin. Plant Biol.* **4**, 494–500 (2001).
35. Choi, K. et al. Arabidopsis homologs of components of the SWR1 complex regulate flowering and plant development. *Development* **134**, 1931–1941 (2007).
36. Lazaro, A., Gomez-Zambrano, A., Lopez-Gonzalez, L., Pineiro, M. & Jarillo, J. A. Mutations in the Arabidopsis SWC6 gene, encoding a component of the SWR1 chromatin remodelling complex, accelerate flowering time and alter leaf and flower development. *J. Exp. Bot.* **59**, 653–666 (2008).
37. March-Diaz, R., Garcia-Dominguez, M., Florencio, F. J. & Reyes, J. C. SEF, a new protein required for flowering repression in Arabidopsis, interacts with PIE1 and ARP6. *Plant Physiol.* **143**, 893–901 (2007).
38. Gomez-Zambrano, A. et al. Arabidopsis SWC4 binds DNA and recruits the SWR1 complex to modulate histone H2A.Z deposition at key regulatory genes. *Mol. Plant* **11**, 815–832 (2018).
39. Choi, K. et al. SUPPRESSOR OF FRIGIDA3 encodes a nuclear ACTIN-RELATED PROTEIN6 required for floral repression in Arabidopsis. *Plant Cell* **17**, 2647–2660 (2005).
40. Deal, R. B., Kandasamy, M. K., McKinney, E. C. & Meagher, R. B. The nuclear actin-related protein ARP6 is a pleiotropic developmental regulator required for the maintenance of FLOWERING LOCUS C expression and repression of flowering in Arabidopsis. *Plant Cell* **17**, 2633–2646 (2005).
41. Martin-Trillo, M. et al. EARLY IN SHORT DAYS 1 (ESD1) encodes ACTIN-RELATED PROTEIN 6 (AtARP6), a putative component of chromatin remodelling complexes that positively regulates FLC accumulation in Arabidopsis. *Development* **133**, 1241–1252 (2006).
42. Ranjan, A. et al. Nucleosome-free region dominates histone acetylation in targeting SWR1 to promoters for H2A.Z replacement. *Cell* **154**, 1232–1245 (2013).
43. Yen, K., Vinayachandran, V. & Pugh, B. F. SWR-C and INO80 chromatin remodelers recognize nucleosome-free regions near +1 nucleosomes. *Cell* **154**, 1246–1256 (2013).
44. Altaf, M. et al. NuA4-dependent acetylation of nucleosomal histones H4 and H2A directly stimulates incorporation of H2A.Z by the SWR1 complex. *J. Biol. Chem.* **285**, 15966–15977 (2010).
45. Babiarz, J. E., Halley, J. E. & Rine, J. Telomeric heterochromatin boundaries require NuA4-dependent acetylation of histone variant H2A.Z in *Saccharomyces cerevisiae*. *Genes Dev.* **20**, 700–710 (2006).
46. Durant, M. & Pugh, B. F. NuA4-directed chromatin transactions throughout the *Saccharomyces cerevisiae* genome. *Mol. Cell Biol.* **27**, 5327–5335 (2007).
47. Galarneau, L. et al. Multiple links between the NuA4 histone acetyltransferase complex and epigenetic control of transcription. *Mol. Cell* **5**, 927–937 (2000).
48. Le Masson, I. et al. Yaf9, a novel NuA4 histone acetyltransferase subunit, is required for the cellular response to spindle stress in yeast. *Mol. Cell Biol.* **23**, 6086–6102 (2003).
49. Zhang, H. et al. The Yaf9 component of the SWR1 and NuA4 complexes is required for proper gene expression, histone H4 acetylation, and Htz1 replacement near telomeres. *Mol. Cell Biol.* **24**, 9424–9436 (2004).
50. Lu, P. Y., Levesque, N. & Kobor, M. S. NuA4 and SWR1-C: two chromatin-modifying complexes with overlapping functions and components. *Biochem Cell Biol.* **87**, 799–815 (2009).
51. Choi, J., Heo, K. & An, W. Cooperative action of TIP48 and TIP49 in H2A.Z exchange catalyzed by acetylation of nucleosomal H2A. *Nucleic Acids Res.* **37**, 5993–6007 (2009).
52. Jarillo, J. A. & Pineiro, M. H2A.Z mediates different aspects of chromatin function and modulates flowering responses in Arabidopsis. *Plant J.* **83**, 96–109 (2015).
53. Crevillen, P. et al. Arabidopsis YAF9 histone readers modulate flowering time through NuA4-complex-dependent H4 and H2A.Z histone acetylation at FLC chromatin. *New Phytol.* **222**, 1893–1908 (2019).
54. Sijacic, P., Holder, D. H., Bajic, M. & Deal, R. B. Methyl-CpG-binding domain 9 (MBD9) is required for H2A.Z incorporation into chromatin at a subset of H2A.Z-enriched regions in the Arabidopsis genome. Preprint at <https://www.biorxiv.org/content/10.1101/404152v1> (2018).
55. Peng, M., Cui, Y., Bi, Y. M. & Rothstein, S. J. AtMBD9: a protein with a methyl-CpG-binding domain regulates flowering time and shoot branching in Arabidopsis. *Plant J.* **46**, 282–296 (2006).
56. Yaish, M. W., Peng, M. & Rothstein, S. J. AtMBD9 modulates Arabidopsis development through the dual epigenetic pathways of DNA methylation and histone acetylation. *Plant J.* **59**, 123–135 (2009).
57. Wei, W. et al. The Alfin-like homeodomain finger protein AL5 suppresses multiple negative factors to confer abiotic stress tolerance in Arabidopsis. *Plant J.* **81**, 871–883 (2015).
58. Deal, R. B., Topp, C. N., McKinney, E. C. & Meagher, R. B. Repression of flowering in Arabidopsis requires activation of FLOWERING LOCUS C expression by the histone variant H2A.Z. *Plant Cell* **19**, 74–83 (2007).
59. March-Diaz, R. et al. Histone H2A.Z and homologues of components of the SWR1 complex are required to control immunity in Arabidopsis. *Plant J.* **53**, 475–487 (2008).
60. Smith, A. P. et al. Histone H2A.Z regulates the expression of several classes of phosphate starvation response genes but not as a transcriptional activator. *Plant Physiol.* **152**, 217–225 (2010).
61. Berg, A. et al. Ten members of the Arabidopsis gene family encoding methyl-CpG-binding domain proteins are transcriptionally active and at least one, AtMBD11, is crucial for normal development. *Nucleic Acids Res.* **31**, 5291–5304 (2003).
62. Greenberg, M. V. et al. Interplay between active chromatin marks and RNA-directed DNA methylation in Arabidopsis thaliana. *PLoS Genet.* **9**, e1003946 (2013).
63. Li, C. et al. The Arabidopsis SWI2/SNF2 chromatin Remodeler BRAHMA regulates polycomb function during vegetative development and directly activates the flowering repressor gene SVP. *PLoS Genet.* **11**, e1004944 (2015).
64. Zhong, X. et al. DDR complex facilitates global association of RNA polymerase V to promoters and evolutionarily young transposons. *Nat. Struct. Mol. Biol.* **19**, 870–875 (2012).
65. Brzezinka, K. et al. Arabidopsis FORGETTER1 mediates stress-induced chromatin memory through nucleosome remodeling. *Elife* **5**, e17061 (2016).
66. Smaczniak, C. et al. Characterization of MADS-domain transcription factor complexes in Arabidopsis flower development. *Proc. Natl Acad. Sci. USA* **109**, 1560–1565 (2012).
67. Dong, J. et al. SLIDE, the protein interacting domain of Imitation Switch remodelers, binds DDT-domain proteins of different subfamilies in chromatin remodeling complexes. *J. Integr. Plant Biol.* **55**, 928–937 (2013).
68. Santisteban, M. S., Kalashnikova, T. & Smith, M. M. Histone H2A.Z regulates transcription and is partially redundant with nucleosome remodeling complexes. *Cell* **103**, 411–422 (2000).
69. Li, G. et al. Imitation Switch chromatin remodeling factors and their interacting RINGLET proteins act together in controlling the plant vegetative phase in Arabidopsis. *Plant J.* **72**, 261–270 (2012).
70. Li, G. et al. ISWI proteins participate in the genome-wide nucleosome distribution in Arabidopsis. *Plant J.* **78**, 706–714 (2014).
71. Bieluszewski, T. et al. AtEAF1 is a potential platform protein for Arabidopsis NuA4 acetyltransferase complex. *BMC Plant Biol.* **15**, 75 (2015).
72. Pfab, A., Bruckmann, A., Nazet, J., Merkl, R. & Grasser, K. D. The Adaptor protein ENY2 is a component of the deubiquitination module of the Arabidopsis SAGA transcriptional co-activator complex but not of the TREX-2 complex. *J. Mol. Biol.* **430**, 1479–1494 (2018).
73. Buenrostro, J. D., Giresi, P. G., Zaba, L. C., Chang, H. Y. & Greenleaf, W. J. Transposition of native chromatin for fast and sensitive epigenomic profiling

of open chromatin, DNA-binding proteins and nucleosome position. *Nat. Methods* **10**, 1213–1218 (2013).

Acknowledgements

We thank Mahnaz Akhavan for support with high-throughput sequencing at the University of California, Los Angeles (UCLA) Broad Stem Cell Research Center BioSequencing Core Facility. Work in the Jacobsen lab was supported by NIH grant R35 GM130272. M.E.P. was supported by the Damon Runyon Cancer Foundation DRG:2217-15. Work in the I.A. laboratory was supported by the National Science Foundation of China (grant numbers: 31571328 and 31870270). S.E.J. is an Investigator of the Howard Hughes Medical Institute.

Author contributions

M.E.P. performed RNA-seq and ChIP-seq and generated sequencing libraries. Y.W. and L.X. developed ARP6-tagged lines and performed IP, co-IP, western blots, RT-PCRs, and genetic analyses. M.E.P. and B.N. developed MBD9-tagged lines. M.E.P., Z.Z. and W.L. performed data bioinformatics analysis. Z.Z. and W.L. performed ATAC-seq. S.F. performed high-throughput sequencing. S.R. and J.A.W. performed mass spectrometry. M.E.P., I.A., and S.E.J. wrote the manuscript. M.E.P., Z.W., I.A. and S.E.J. coordinated the research.

Additional information

Supplementary Information accompanies this paper at <https://doi.org/10.1038/s41467-019-11291-w>.

Competing interests: The authors declare no competing interests.

Reprints and permission information is available online at <http://npg.nature.com/reprintsandpermissions/>

Peer review information: *Nature Communications* thanks the anonymous reviewers for their contribution to the peer review of this work.

Publisher's note: Springer Nature remains neutral with regard to jurisdictional claims in published maps and institutional affiliations.



Open Access This article is licensed under a Creative Commons Attribution 4.0 International License, which permits use, sharing, adaptation, distribution and reproduction in any medium or format, as long as you give appropriate credit to the original author(s) and the source, provide a link to the Creative Commons license, and indicate if changes were made. The images or other third party material in this article are included in the article's Creative Commons license, unless indicated otherwise in a credit line to the material. If material is not included in the article's Creative Commons license and your intended use is not permitted by statutory regulation or exceeds the permitted use, you will need to obtain permission directly from the copyright holder. To view a copy of this license, visit <http://creativecommons.org/licenses/by/4.0/>.

© The Author(s) 2019